Bilinear pressure diffusion and termination of bilinear flow in a vertically fractured well injecting at constant pressure

Patricio-Ignacio Pérez D.[1], Adrián-Enrique Ortiz R.[2], Ernesto Meneses Rioseco[3]

[1]Department of Mechanical Engineering, Universidad Técnica Federico Santa María, Valparaíso, 2340000, Chile
5   [2]Department of Chemical and Environmental Engineering, Universidad Técnica Federico Santa María, Valparaíso, 2340000, Chile
[3]Department of Geothermics and Information Systems, Leibniz Institute for Applied Geophysics, Hannover, 30655, Germany

Correspondence to: Adrián-Enrique Ortiz R. (adrian.ortiz@usm.cl)

10   **Abstract.** This work studies intensively the flow in fractures with finite hydraulic conductivity intersected by a well injecting/producing at constant pressure. Previous investigations showed that for a certain time the reciprocal of flow rate is proportional to the fourth root of time, which is characteristic of the flow regime known as bilinear flow. Using a 2D numerical model, we demonstrated that during the bilinear flow regime the transient propagation of isobars along the fracture is proportional to the fourth root of time. Moreover, we present relations to calculate the termination time of bilinear flow under constant injection or production well pressure, as well as, an expression for the bilinear hydraulic diffusivity of fractures with finite hydraulic conductivity. To determine the termination of bilinear flow regime, two different methods were used: (a) numerically measuring the transient of flow rate in the well and (b) analyzing the propagation of isobars along the fracture. Numerical results show that for low fracture conductivities the transition from bilinear flow to another flow regime occurs before the pressure front reaches the fracture tip and for high fracture conductivities it occurs when the pressure front arrives at the fracture tip. Hence, this work complements and advances previous research on the interpretation and evaluation of well test analysis under different reservoir conditions. Our results aim at improving the understanding of the hydraulic diffusion in fractured geologic media and as a result they can be utilized for the interpretation of hydraulic tests, for example to estimate the fracture length.

25   **Keywords:** Bilinear flow; Rate transient analysis; Hydraulic diffusivity; Pressure diffusion; Porous geologic media.

Highlights

- The reciprocal of flow rate is proportional to the fourth root of time
- The migration of isobars in the fracture is proportional to the fourth root of time
- For low fracture conductivities, bilinear flow ends before the pressure front reaches the fracture tip
30   - For high fracture conductivities, bilinear flow ends when the pressure front reaches the fracture tip
- Isobars accelerate when they approach to the fracture tip

1 Introduction

Understanding the different flow regimes in fractured reservoirs has always been key in the interpretation and evaluation of hydraulic well tests as well as in the production optimization of reservoirs. An in-depth description of the behavior of

35   multiple flow regimes in fractures is extremely important to master the physics behind the modeling and simulation and, hence, to reliably interpret the results. Models considering a double porosity were first examined by Barenblatt et al. (1960). They introduced the basics of fluid dynamics in fissured rocks by deriving general equations of the seepage of liquid in porous media, taking into consideration its double-porosity condition. Cinco-Ley and Samaniego-V. (1981) differentiated clearly four flow regimes: fracture linear flow, bilinear flow (for the first time named in this way by them), formation linear

40   flow and pseudo-radial flow.

Usually, reservoir properties are obtained from well test or production data at a constant flowrate (pressure transient analysis). However, in some cases, reservoir production is performed at a constant pressure. This is illustrated, for instance, by the case where fluid is produced from the reservoir by means of a separator or constant-pressure pipeline (e.g., gas wells; Ehlig-Economides, 1979). Open wells flow at constant atmospheric pressure, e.g., artesian water wells. Geothermal fluid

45   production may propel a back-pressure steam turbine, where steam leaves the turbine at the atmospheric pressure or at a higher constant pressure. Other operational conditions that require to maintain a constant pressure are encountered in gas wells, where a fixed pressure must be maintained for sales purposes or in water injection wells, where the injection pressure is constant (Da Prat, 1990). In addition, reservoir production at constant pressure is conducted during rate decline periods of reservoir depletion (Da Prat, 1990; Ehlig-Economides, 1979). Although the interpretation of data collected in well tests and

50   production at constant flowrate (pressure transient analysis) has considerably improved, the rate transient analysis has not experienced such development (Houzé et al., 2018). Lately, a significant interest for the rate transient analysis has increased, which is attributed to the exploitation of unconventional hydrocarbon plays due to the extremely slow and long transient responses (Houzé et al., 2018). The production from unconventional plays has recently been made possible by creating fractures, which has strengthened the importance of having better tools and methods that allow to obtain information of the

55   fractures considering either the transient analysis of pressure or flow rate or the combination of both. It is exceedingly difficult to maintain a constant flow rate during long times, especially in low permeability formations as in the case of unconventional plays (Kutasov and Eppelbaum, 2005). It is worth mentioning that constant-pressure tests have the advantage of minimizing changes in the wellbore storage coefficient (Earlougher Jr., 1977). The wellbore storage effects distort early-time pressure evolution, subsequently, the constant-pressure well tests allow the analysis of early-time data and in this way

60   information of the reservoir in the vicinity of the wellbore can be obtained (Nashawi and Malallah, 2007). Moreover, rate-transient tests are particularly suitable for the illustration of the long-term behavior of formations (Torcuk et al., 2013). Conceivably one of the main reasons why constant pressure tests is not a more common technique in reservoir engineering arises from the fact that in some cases no analytical solutions are available for the pressure diffusion equation (Kutasov and Eppelbaum, 2005).

65

Arps (1945) presented an empirical production correlation for the rate history of a well during the boundary-dominated flow regime. Later, Locke and Sawyer (1975) generated type-curves for a vertically fractured reservoir producing at constant pressure with the objective of characterizing the behavior of flow rate. In this context, Agarwal et al. (1979) presented type-curves to analyze the early time cases. In addition, they determined the fracture conductivity T_D by means of
70   graphing the logarithm of the reciprocal of flow rate vs. the logarithm of time and utilizing type-curve matching techniques. Fetkovich (1980) introduced the rate decline analysis in the radial-flow system, similar to pressure transient analysis, however, only applicable to circular homogeneous reservoirs.

Guppy et al. (1981a) studied the effect of non-Darcy flow within a fracture. They concluded that the fracture conductivity T_D has an apparent conductivity that is not constant over time. Subsequently, a major contribution was made by Guppy et al.
75   (1981b), which consisted of presenting semi-analytical solutions for bilinear flow - both works considered constant pressure production. They demonstrated that the reciprocal of dimensionless flow rate is proportional to the fourth root of dimensionless time when producing at constant wellbore pressure. Guppy et al. (1988) contributed further to the previous works investigating deeply the cases with turbulent flow in the fracture and for the first time they examined a technique that concerns both buildup and drawdown data when the well is producing at constant pressure. Subsequently, a direct method to
80   estimate the turbulent term considering high-velocity flow in variable rate tests was documented by Samaniego-V. and Cinco-Ley (1991). In addition, Berumen et al. (1997) developed a transient pressure analysis under both constant wellhead and bottom-hole pressure conditions considering high-velocity flow. Wattenbarger et al. (1998) presented decline curve analysis methods for tight gas wells producing at constant pressure with long-term linear behavior (fracture flow). Pratikno et al. (2003) prepared rate-time decline curves for fractured wells producing at constant pressure, including fracture lineal
85   and bilinear flow. Follow-up investigations conducted by Nashawi (2006) presented semi-analytical solutions when considering non-Darcy flow in a fracture and a method with which it is possible to quantify the turbulence in a fracture. Nashawi and Malallah (2007) developed a direct method to determine the fracture and reservoir parameters without having to use type-curve matching techniques. In this context, Heidari Sureshjani and Clarkson (2015) concluded that plotting techniques overestimate the fracture half-length, leading them to the formulation of an analytical methodology with which it
90   is estimated more precisely.

Recently, Silva-López et al. (2018) introduced a new method to obtain Laplace-transformed solutions and as a result they predicted new regions of flow behavior. This latter method is documented for injecting at either constant flow rate or pressure. In addition, the theory of well testing has been improved by investigating the effects of non-uniform properties of hydraulic fractures (He et al., 2018). Moreover, Wang et al. (2018) presented an enhanced model to simulate the
95   productivity of volume fractured wells and Dejam et al. (2018) documented a new semi-analytical solution applicable in dual-porosity formations.

When it comes to studying the termination of bilinear flow regime and the spatiotemporal propagations of isobars, there is not much evidence of investigations considering injection or production at constant pressure. To the best of our knowledge,

it has only been investigated when injecting at constant flow rate in the well (Cinco-Ley and Samaniego-V., 1981; Weir,

100   1999). In this regard, new criteria to determine the end of bilinear flow, which are also used in this investigation, were

introduced by Ortiz R. et al. (2013).

This work addresses the challenging task of gaining a quantitative understanding of bilinear flow from rate transient

analysis for wells producing at constant pressure, requiring a multidisciplinary approach. Expanding the understanding of

bilinear flow regime in fractured reservoirs leads to a more precise analysis of well tests and production or injection data.

105   This, in turn, makes it possible to characterize a reservoir more accurately and consequently have more reliable assessments

of its behavior, leading to better concepts of production optimization during operation.

Taking into account injection at constant pressure, this investigation presents for the first time: (a) the propagation of

isobars P_N along the fracture and the formation during bilinear flow regime, as well as the computation of the bilinear

hydraulic diffusivity of fracture; and (b) the study of termination of bilinear flow regime utilizing criteria previously

110   presented and a criterion firstly documented here.

2 Background

2.1 Governing equations and parameters

This study is carried out considering that single-phase fluid in both matrix and fracture obeys the Darcy's law in a two-

dimensional confined and saturated aquifer. The selected software-simulator for ~~numerically modeling groundwater flow~~ in

115   the reservoir is COMSOL Multiphysics. ~~For the matrix, the~~ equation utilized to describe the hydraulics of compressible

Newtonian fluid in a ~~fractured~~ reservoir is given by:

$$s_m \frac{\partial p}{\partial t} = \frac{k_m}{\eta_f} \left(\frac{\partial^2 p}{\partial x^2} + \frac{\partial^2 p}{\partial y^2} \right), \tag{1}$$

where s_m (Pa^{-1}) represents the specific storage capacity of matrix, k_m (m^2) the matrix permeability, η_f (Pa s) the dynamic

fluid viscosity and p (Pa) the fluid pressure. For the fracture, the equation is given by:

120    $$s_F b_F \frac{\partial p}{\partial t} = \frac{T_F}{\eta_f} \frac{\partial^2 p}{\partial x^2} + \frac{q_F(x,t)}{h}, \tag{2}$$

where s_F (Pa^{-1}) represents the specific storage capacity of fracture, b_F (m) the aperture of fracture, T_F (m^3) the fracture

conductivity, h (m) the fracture height and $q_F(x,t)$ the fluid flow between matrix and fracture (see Cinco L. et al., 1978 and

Guppy et al., 1981b). In this study, s_F is neglected because we assume that the fracture is non-deformable and the amount of

fluid in the fracture is small enough to consider its compressibility as negligible. Thus, Eq. (2) reads:

125    $$\frac{T_F}{\eta_f} \frac{\partial^2 p}{\partial x^2} + \frac{q_F(x,t)}{h} = 0. \tag{3}$$

The pressure diffusion equations for matrix and fracture are coupled by the term $q_F(x,t)$, which is defined as:

$$\frac{q_F(x,t)}{h} = 2\frac{k_m}{\eta_f}\frac{dp}{dy}\bigg|_{y=0}, \tag{4}$$

where the factor 2 relates to the contact between matrix and fracture via its two surfaces.

2.2 Dimensionless parameters

130   This study is conducted using dimensional properties but the analysis of results is performed utilizing the conventional dimensionless definitions. The dimensionless flow rate is given by:

$$\frac{1}{q_{wD}} = \frac{k_m h(p_w - p_i)}{q_w \eta_f}, \tag{5}$$

where q_w (m³ s⁻¹) represents the flow rate in the well, q_{wD} the dimensionless flow rate in the well, h (m) the fracture height, p_i (Pa) the initial pressure of the formation and fracture, and p_w (Pa) the constant injection pressure.

135   The dimensionless fracture conductivity is defined as:

$$T_D = \frac{T_F}{k_m x_F}, \tag{6}$$

where $T_F = k_F b$ (m³) denotes the fracture conductivity and x_F (m) the fracture half-length.

Instead of using the conventional definition of dimensionless time $t_D = tD_m/x_F^2$, we prefer to use a modified definition presented by Ortiz R. et al. (2013):

140    $$\tau = \frac{t_D}{T_D^2} = \frac{D_m k_m^2}{T_F^2}t, \tag{7}$$

where $D_m = k_m/(\eta_f s_m)$ (m² s⁻¹) represents the hydraulic diffusivity of matrix and τ the dimensionless time. Finally, the dimensionless x-coordinate, which corresponds to the fracture axis (see Fig. 1), is defined as:

$$x_D = \frac{x}{x_F}; \tag{8}$$

and the dimensionless y-coordinate, that represent the axis perpendicular to the fracture (see Fig. 1), is defined as:

145    $$y_D = \frac{y}{x_F}. \tag{9}$$

2.3 Previous solutions for bilinear flow at constant wellbore pressure

As mentioned earlier, bilinear flow regime was firstly documented by Cinco-Ley and Samaniego-V. (1981). According to their proposed definition, it consists of an incompressible linear flow within the fracture and a slightly compressible linear flow in the formation. Moreover, a semi-analytic solution for a vertically fractured well producing at constant pressure

150   during bilinear flow regime was presented by Guppy et al. (1981b). They demonstrated that the reciprocal of flow rate is proportional to the fourth root of time and the governing equation is given in dimensionless form by:

$$\frac{1}{q_{wD}}(\tau) = \frac{\pi \Gamma(3/4)}{\sqrt{2T_D}} t_D^{1/4} \cong 2.722\tau^{1/4}. \tag{10}$$

Silva-López et al. (2018) presented an analytical solution for an infinite fracture considering the case of variable flow rate for long-time in dimensionless form:

155
$$\frac{1}{q_{wD}}(t_D) = \frac{1}{f(t_D)}\frac{\pi^{1/4}\sqrt{T_D}}{2\delta}t_D{}^{1/4}.$$
(11)

Note that Eq. (11) is written in the notation used in this paper. $f(t_D)$ represents a function that describes the transient behavior of pressure in the well and δ denotes a constant.

2.4 Description of the model

The two-dimensional model set up in this work is composed of a vertical fracture embedded in a confined horizontal
160 reservoir. The matrix and fracture are porous geologic media considered saturated, continuous, isotropic and homogeneous. The gravity effects are neglected. Fluid flow enters or abandons the matrix-fracture system only through the well. This investigation is symmetric, i.e. the flow rate calculated in the well q_w corresponds to the half of total flow rate for the case of studying the complete fracture length (see Fig. 1). The pressure in the well p_w is set to 10^6 Pa during the entire simulation and the initial conditions for pressure in the reservoir and the fracture p_i is set to 10^5 Pa. We use these pressure conditions in
165 order to ensure an injection of fluid from the well to the matrix-fracture system. The order of magnitude of $(p_w - p_i)$ is similar to that utilized by Nashawi and Malallah (2007). No-flow boundary conditions are assigned to the boundaries of the reservoir since it is considered as confined. In order to ensure that the boundary conditions do not affect the modeling outcome, the system size was consecutively enlarged to double, triple and quadruple, and the results were compared to each other and, in fact, they were identical. During the entire simulation the following parameters remained constant: $k_m = 1 \cdot$
170 10^{-18} m² , $k_F = 1.5 \cdot 10^{-13}$ m², $s_m = 1 \cdot 10^{-11}$ Pa⁻¹, $b_F = 1 \cdot 10^{-3}$ m and $\eta_f = 2.5 \cdot 10^{-4}$ Pa s. Similarly as in Ortiz R. et al. (2013), the fracture half-length takes different values from 1.5 m up to 1500 m with the objective of varying the dimensionless fracture conductivity T_D from 0.1 up to 100 (see Eq. 6). The time steps used in these numerical simulations were 0.01 s from the start until the first 40 s, 20 s from 40 s until 600 s, 60 s from 600 s until 12.000 s, 300 s from 12000 s until 72000 s, 1000 s from 72000 s until $5 \cdot 10^5$ s and $5 \cdot 10^5$ s from $5 \cdot 10^5$ s until $2 \cdot 10^8$ s (or until $6 \cdot 10^8$ s employed
175 for the master curve, Fig. 2).

The mesh is comparatively fine in the vicinity of the fracture and the well and it becomes coarser when moving away from the fracture, since there is an extremely large hydraulic gradient near the fracture and the well (see Fig. 1b). The minimum element size is 0.0045 m near the well, the maximum element size is 80 m close to the boundaries of the reservoir and the maximum element growth rate is 1.3 m. The number of elements varies according to the different size and mesh
180 structure used to describe the respective model scenario. The minimum and maximum number of elements is 12929 and 1358697, respectively.

3 Results

Numerical simulations ~~computed~~ show that during an interval of time the reciprocal of dimensionless flow rate in the well $1/q_{wD}$ is proportional to the fourth root of dimensionless time $\tau^{1/4}$ (Fig. 2). This proportionality is in accordance with the behavior documented by Guppy et al. (1981b) and Silva-López et al. (2018). In particular, we can describe the variation of dimensionless flow rate in the well during the bilinear flow regime as:

$$\frac{1}{q_{wD}}(\tau) = A \cdot \tau^{1/4}, \tag{12}$$

where the constant $A = 2.60$. From now on, we will refer to this equation as bilinear-fit-curve (grey line in Fig. 2). Note that the coefficient A obtained by Guppy et al. (1981b) employing a semi-analytical solution is approximately $A = 2.722$ (see Eq. 10). This slight difference between our and their result for A might be due to the temporal and spatial discretization utilized by them. This issue is discussed in the next subsection of this paper. The reciprocal of dimensionless flow rate exhibits a behavior proportional to the fourth root of time (Eq. 12), which is characteristic of bilinear flow regime, hence we can corroborate the occurrence of it.

We define the master curve as the one that describes the behavior of an infinitely long fracture (red line in Fig. 2). The curves describing the behavior of the reciprocal of dimensionless flow rate over time for different fracture conductivities, from $T_D = 0.1$ up to $T_D = 100$, are addressed as type-curves (black lines in Fig. 2).

Taking into account all the aspects previously described, when type-curves start departing from the bilinear-fit-curve (Fig. 2), this indicates that the transition from bilinear flow regime to formation linear flow regime (cases with high T_D) or to pseudo-radial flow regime (cases with low T_D) begins (Ortiz R. et al., 2013).

3.1 Propagation of isobars along the fracture and the formation

In order to characterize the different isobars, the following definition is used (Ortiz R. et al., 2013):

$$P_N = \frac{p(x, y, t) - p_i}{p_w - p_i}, \tag{13}$$

where $p(x, y, t)$ denotes the pressure at the position (x, y) in the fracture or the matrix at time t. The values of P_N utilized in this study are 0.01 and 0.05, which are equivalent to the isobars 109 kPa and 145 kPa, respectively.

The results of this investigation show that initially the migration of isobars P_N along the fracture (see Fig. 1) is proportional to the fourth root of time:

$$x_{iD} = \alpha_b T_D \tau^{1/4}, \tag{14}$$

where x_{iD} represents the dimensionless distance of normalized isobars P_N from the well along the x_D axis and α_b is a constant depending on the studied isobar P_N (see Fig. 3).

In addition, the migration of isobars P_N in the matrix (perpendicular to the fracture and at $x_D = 0$, see Fig. 1) for short times may be described by:

$$y_{iD} = \alpha_m T_D \tau^{1/2}, \tag{15}$$

where y_{iD} denotes the dimensionless distance of normalized isobars P_N from the well along the y_D axis and α_m is a constant for pressure diffusion in the matrix, ~~respectively~~ depending on the isobar under investigation.

215   When expressing equations (14) and (15) in dimensional form, for the x axis Eq. (14) is given by:

$$x_i(t) = \alpha_b (D_b t)^{1/4}; \tag{16}$$

and for the y axis Eq. (15) is given by:

$$y_i(t) = \alpha_m (D_m t)^{1/2}. \tag{17}$$

In the Eq. (17), $D_m = k_m/(\eta_f s_m)$ (m^2 s^{-1}) is known as hydraulic diffusivity of matrix and is analogue to the definition of

220   thermal diffusivity. Additionally, in the Eq. (16) $D_b = T_F^2 / k_m \eta_f s_m$ (m^4 s^{-1}) is referred to as effective hydraulic diffusivity of fracture during bilinear flow regime (Ortiz R. et al., 2013).

The numerical results are specified as migration-type-curves (see black lines in Figs. 3, 4 and 5) and the fit equations for the propagation of isobars are referred to as migration-fit-curves (see grey lines in Figs. 3, 4 and 5). It can be qualitatively noticed throughout the cases under study that for low fracture conductivities, i.e. $T_D = 0.1$ and $T_D = 0.3$, the migration-type-

225   curves, which describe the migration of isobars P_N along both x_D and y_D axis, start departing from migration-fit-curves before the studied isobars reach the fracture tip (Figs. 3 a, b, c, d, and Fig. 4). In contrast, for the cases considering high fracture conductivities, i.e. $T_D = 1.1$, $T_D = 6.3$ and $T_D = 9.4$, there is no qualitative evidence of migration-type-curves departing from migration-fit-curves before the studied isobars P_N arrive at the fracture tip (Figs. 3 e, f, g, h, i, j and Fig. 4). The latter results, however, show some exceptions for a slight acceleration exhibited by the isobars P_N when they are

230   reaching the fracture tip. It is important to mention that this relatively small acceleration also occurs for cases with low fracture conductivities (see Figs. 3c and 3d). The same behavior was observed by Ortiz R. et al. (2013) for the injection at constant flow rate.

On the one hand, when discussing qualitatively about the early time we notice that the higher the value of the isobar P_N the sooner it migrates proportional to the fourth root of time (Fig. 5). For example, at the same time ($\tau = 5 \cdot 10^{-10}$) the isobar

235    $P_N = 0.66$ (the greater isobar under investigation) starts to migrate along the fracture proportional to the fourth root of time whereas the isobar $P_N = 0.01$ (the smaller isobar under study) has not yet started to propagate proportional to the fourth root of time. Moreover, the greater the isobar P_N the shorter its distance from the well x_{iD} in comparison to other smaller isobars when considering the same time τ, which is logical since the isobars migrate one after the other. On the other hand, when discussing qualitatively about the long time, we notice that the smaller isobar $P_N = 0.01$ departs from the migration-fit-curve

240   when it reaches the fracture tip. In contrast, the greater isobar $P_N = 0.66$ departs from the migration-fit-curve before its arrival at the fracture tip (Fig. 5). Additionally, it can be seen that the higher the value of isobar P_N the farthest from the fracture tip or, closer to the well, it starts departing from the migration-fit-curve. Thus, taking into consideration the migration of isobars, it is reasonable to conclude that for high fracture conductivities T_D the bilinear flow regime ends when the pressure front reaches the fracture tip.

245   Previously, we referred to the observation concerning the acceleration that isobars experience when they are arriving at the fracture tip (see Figs. 3 and 5), which was also documented in Ortiz R. et al. (2013) for the case of fluid injection at constant flow rate. To prove that it is truly an acceleration, the velocity of isobars is determined by calculating $\Delta x_{iD}/\Delta \tau$ and it is graphed versus time τ as well as versus the distance of isobars from the well x_{iD} (see Fig. 6). The existence of this acceleration in $x_{iD} = 1$ (fracture tip, see Fig. 6) can be clearly noticed. The velocity of isobars v_{iD} during their migration

250   along the fracture decreases almost for the complete intervals of time considered (Figs. 6a and 6c), except for its evident increase at times when isobars are reaching the fracture tip. The velocity of isobars can be described within the intervals of time used as:

$$v_{iD}(\tau) = \beta_b T_D \tau^{-3/4}, \tag{18}$$

where β_b is a constant depending on the isobar under study. The velocity of isobars in terms of their distances from well and

255   within the ranges of distance used can be described as:

$$v_{iD}(x_{iD}) = \gamma_b T_D x_{iD}^{-3}, \tag{19}$$

where γ_b is a constant depending on the isobar under study.

Before the isobars reach the fracture tip and at the same time τ the velocity of isobar $P_N = 0.01$ is higher than the velocity of $P_N = 0.05$ (Figs. 6a and 6c). Furthermore, we can see that the arrival at the fracture tip of $P_N = 0.05$ occurs after the

260   arrival of $P_N = 0.01$, what is also distinguishable in Figs. 3 and 5. The latter modeling results make sense since isobars migrate one after the other, being the smaller of them $P_N = 0.01$ first in the propagation along the fracture. Moreover, before the arrival of isobars at the fracture tip and at a certain point belonging to the fracture the velocity of the isobar $P_N = 0.01$ is higher than the velocity of $P_N = 0.05$ (Figs. 6b and 6d).

3.2 Termination of bilinear flow

265   Concerning the study related to the termination of bilinear flow considering fluid injection at constant flow rate, Ortiz R. et al. (2013) introduced three criteria: the transition criterion, the reflection criterion and the arrival criterion. The transition and reflection criteria consider data regarding the well and the arrival criterion considers data related to the migration of isobars P_N along the fracture. In this work, is presented for the first time the fracture criterion, which considers data related to the propagation of isobars along the fracture. To sum up, we can say that there exist two methodologies to quantify the

270   termination of bilinear flow: (a) considering the transient of pressure/flow rate in the well and (b) considering the propagation of isobars P_N along the fracture.

3.2.1 Transition criterion

This criterion quantifies the clockwise deviation of type-curves from the bilinear-fit-curve in Fig. 2 and it is fundamentally utilized for low fracture conductivities:

275
$$\varepsilon = 1 - \left(\frac{\frac{1}{q_{wDt}}}{2.60\tau^{\frac{1}{4}}} \right),$$
(20)

where q_{wDt} represents the dimensionless flow rate of type-curves (Fig. 2). The cases that are under the study of the transition criterion are not affected by the fracture tip and the termination time is similar for all type-curves for which this criterion is applicable (see τ_t in Fig. 7).

3.2.2 Reflection criterion

280   It quantifies the counterclockwise deviation of type-curves from the master curve in Fig. 2 due to their reflection at the fracture tip (Ortiz R. et al., 2013) and it is used for high fracture conductivities:

$$\varepsilon = 1 - \left(\frac{\frac{1}{q_{wD\infty}}}{\frac{1}{q_{wDt}}} \right) = 1 - \left(\frac{q_{wDt}}{q_{wD\infty}} \right),$$
(21)

where $q_{wD\infty}$ denotes the dimensionless flow rate of the master curve (Fig. 2). The cases that are under the study of this criterion are affected by the fracture tip, hence the higher T_D the shorter the termination time (see τ_r in Fig. 7).

285   3.2.3 Arrival criterion

It represents the moment at which the isobars arrive at the fracture tip. The cases that are under the study of this criterion are affected by the fracture tip, hence the higher T_D the shorter the termination time (see τ_a in Fig. 7).

3.2.4 Fracture criterion

Basically, it states that the separation between the migration-type-curves and the migration-fit-curves (see Fig. 3) is 290   representative of the end of bilinear flow regime and it is applicable to low fracture conductivities. In this work, the propagation along y_D is not a criterion for the termination of bilinear flow, it is only a contribution to the study of its behavior. Usually, for the analysis of bilinear flow at constant injection or production flow rate the transient wellbore pressure is studied, thus the bilinear flow occurs when the wellbore pressure is proportional to the fourth root of time (Cinco-Ley and Samaniego-V., 1981; Ortiz R. et al., 2013; Weir, 1999). Similarly, for constant wellbore pressure as in this work, 295   the bilinear flow can be recognized by the proportionality between $1/q_{wD}$ and $\tau^{1/4}$. The fracture criterion, instead of using the transients of $1/q_{wD}$ it quantifies the separation of migration-type-curves from migration-fit-curves (Fig. 3) and is defined as:

$$\varepsilon = 1 - \left(\frac{x_{iDf}}{x_{iDt}} \right),$$
(22)

where x_{iDt} denotes the propagation x_{iD} of migration-type-curves and x_{iDf} represents the propagation x_{iD} of migration-fit-300   curves. The latter have the form $\alpha_b T_D \tau^{1/4}$ (see Eq. 14 and Fig. 3). The cases that are under the study of the fracture criterion

are not affected by the fracture tip and the termination time is similar for all migration-type-curves for which this criterion is applicable (see τ_F in Fig. 7). Summarizing, this criterion takes into consideration only the movement of isobars P_N along the fracture and not the change of $1/q_{wD}$ in the well, and it is suitable for low fracture conductivities T_D.

305   In the framework of this study, when we consider the ~~transient~~ of flow rate in the well, the criteria that can be utilized are the transition criterion (see section 3.2.1) and the reflection criterion (see section 3.2.2). When we consider the propagation of isobars along the fracture, the criteria that can be used are the arrival criterion (see section 3.2.3) and the fracture criterion (see section 3.2.4).

Despite the values for the transition criterion and the fracture criterion are different, their behaviors are similar. They present almost constant values within the range of T_D in which these criteria are applied. Note that the values of fracture

310   criterion are always higher than the values of transition criterion. The fracture criterion can give us a reliable estimate of the termination of bilinear flow when considering the low fracture conductivities T_D for which this criterion is applicable. The transition and fracture criteria make sense only until the isobars P_N reach the fracture tip (see Fig. 7).

As we exposed earlier, it does not make sense to discuss about the occurrence of bilinear flow after the pressure front has already arrived at the fracture tip. Nevertheless, the results show (Fig. 7) that the reflection time τ_r (related to the flow rate

315   calculated in the well) is greater than the arrival time τ_a (related to the moment at which the isobars reach the fracture tip). It means that the reciprocal of dimensionless flow rate calculated in the well is proportional to the fourth root of time even when the pressure front has already reached the fracture tip. This aspect is discussed afterward in a subsequent section in more detail.

4 Discussion

320   The dimensionless time was not defined using the conventional definition t_D but a modified definition τ presented by Ortiz R. et al. (2013). It turned out to be convenient in terms of interpreting the results for bilinear flow since it was possible to graph the behavior of $1/q_{wD}$ vs. τ for all fracture conductivities T_D in the same graph (Fig. 2).

As for the comparison between the coefficient $A = 2.60$ obtained by us (Eq. 12) and the coefficient $A = 2.772$ documented by Guppy et al. (1981b), we can observe a discrepancy between ~~both~~ results of approximately 6%. This

325   discrepancy can be considered rather low. This difference could be attributed to the spatial and temporal discretization utilized in our work, which is more sophisticated than the discretization used by Guppy et al. (1981b).

Some type-curves bend clockwise and some other bend counterclockwise from bilinear-fit curve (Fig. 2). Among the cases of fracture conductivities T_D studied, the type-curves that bend clockwise are $T_D = 0.1, 0.3$ and 1.1, and those that bend counterclockwise are $T_D = 3.1, 6.3, 9.4, 20, 31, 50$ and 100. Similar results were obtained by Ortiz R. et al. (2013) for

330   the case of injection at constant flow rate. For the interval of time utilized in the simulation, the behavior of $1/q_{wD}$ versus τ for fracture conductivities $T_D = 0.1$ and 0.3 is identical to the behavior of an infinitely long fracture (master curve, red line

in Fig. 2) since the separation of the mentioned type-curves from the master curve shall occur at time greater than the simulation time utilized here.

335   Our results concerning the propagation of isobars along the fracture and the matrix (Eqs. 14 and 15) are similar to the results previously presented by Ortiz R. et al. (2013) regarding the migration of isobars. The values of α_b obtained by us for $P_N = 0.01$ and 0.05 are quantitatively different from the values documented by them in 4.6% and 5.8%, respectively.

    At times when isobars are reaching the fracture tip they exhibit an acceleration along the fracture (see Figs. 3 and 5). Subsequently, after arriving at the fracture tip, their progress along the fracture keep relatively constant. Afterward, they experience another acceleration along the fracture with which the migration of isobars seems to approach to a propagation

340   proportional to the square root of time (see Fig. 3). An identical behavior was observed by Ortiz R. et al. (2013) and they attributed it to the reflection of isobars at the fracture tip, which makes sense and could be confirmed in this study. The acceleration nearby the fracture tip can be observed more clearly when analyzing the velocity along the fracture (see Figs. 6b and 6d). During the intervals of time used, the migration of isobars along the fracture experiences a constant deceleration, except when they approach to the fracture tip. This deceleration is qualitatively identical for $P_N = 0.01$ and $P_N = 0.05$ (see

345   Figs. 6a and 6c). It is evident that for all fixed dimensionless positions in the fracture and considering the same fracture conductivity T_D, the velocity v_{iD} is higher for low values of normalized isobars p_N (see Figs. 6b and 6d). One reason of this observation is that once the deceleration begins, $P_N = 0.01$ propagates faster than $P_N = 0.05$ since the initial velocity (when the isobar leaves the well) of the isobar $P_N = 0.01$ is higher than initial velocity of the isobar $P_N = 0.05$. This behavior is explained based on the fact that the pressure gradient between the well and the fracture is bigger when $P_N = 0.01$ is leaving

350   the well than when $P_N = 0.05$ is leaving it. Furthermore, for all fixed dimensionless positions in the fracture and considering the same isobar P_N, the velocity v_{iD} is higher for high fracture conductivities (see Figs. 6b and 6d).

    Using Eq. (18) and Eq. (19) the migration of isobars along the fracture can be described as:

$$x_{iD} = \left(\frac{\beta_b}{\gamma_b}\right)^{-1/3} \tau^{1/4}. \tag{23}$$

Note that Eq. (23) has the same form that Eq. (14), thus:

355
$$\left(\frac{\beta_b}{\gamma_b}\right)^{-1/3} = \alpha_b T_D. \tag{24}$$

It is possible to verify the validity of Eq. (24) by introducing the required values.

    For the case of injection at constant flow rate the results obtained by Ortiz R. et al. (2013) for the arrival time, the reflection time and the transition time are similar to ours (see Table 1).

    When it comes to the criteria that consider the transient of $1/q_{wD}$ some observations can be made: (a) in the case of Fig.

360   7a the transition criterion is fulfilled up to a value of T_D approximately 2 and for values of T_D above 3 the reflection criterion is fulfilled; and (b) in the case of Fig. 7b the transition criterion is fulfilled up to a value of T_D approximately 1.1 and for values of T_D above 2 the reflection criterion is fulfilled. Note that for the case ε and $P_N = 0.01$ and for $2 < T_D < 3$ as well as for the case ε and $P_N = 0.05$ and for $1.1 < T_D < 2$, it is not clear what happens with the transition criterion since it seems

that the values converge to the fit-curve for the reflection criterion (see Fig. 7). A deeper study is required to determine more
365   precisely what occurs within those ranges of T_D. Ortiz R. et al. (2013) concluded the same based on their work.

Finally, there are two ways to determine the termination of bilinear flow: (I) by numerically measuring the transient flow
rate in the well and obtaining the transition time τ_t for low T_D and the reflection time τ_r for high T_D and (II) according to the
migration of isobars along the fracture (not measurable in the well), obtaining the fracture time τ_F for low T_D and the arrival
time for high T_D (see Table 2).

4.1 Application to well testing problems

In practical terms, when analyzing the transient flow rate in a well only the transition time τ_t and the reflection time τ_r
can be determined. The transition time defines the end of bilinear flow when $1/q_w$ is no longer proportional to $t^{1/4}$, and the
reflection time refers to the moment at which a variation of pressure is evident in the fracture tip. With the current field
methods, it is not possible to determine the termination of bilinear flow utilizing the progress of the pressure front along the
375   fracture, although this is more physically reasonable. Nevertheless, the fracture length can be constrained indirectly, for
instance by computing the time at which the pressure arrives at the fracture tip and its relation with respect to the reflection
time. The relation between the arrival time τ_a and the reflection time τ_r is given by:

$$\tau_a \cong 0.0579\tau_r \tag{25}$$

for ε and $P_N = 0.01$ (see Fig. 7a); and

380    $$\tau_a \cong 0.0736\tau_r \tag{26}$$

for ε and $P_N = 0.05$ (see Fig. 7b).

In the following, we present two artificial cases in which synthetic curves were constructed to illustrate how the
measurements of the flow rate in wells during hydraulic tests at constant pressure are used to estimate or restrict the length of
fractures with finite hydraulic conductivity (bilinear flow). The synthetic curves are not obtained from measurements of
385   realistic well tests but computed utilizing the validated porous and fracture model included in COMSOL Multiphysics and in
previous papers.

4.1.1 Case 1: high dimensionless fracture conductivities T_D

We proceed to elaborate a method to estimate the fracture length using measurements of the flow rate in the well. This is
motivated by its usefulness for cases with high T_D in which the reflection criterion is applicable, i.e., provided that the isobar
390   that is under study reaches the fracture tip while bilinear flow is still in progress. In this example, the values of the
dimensional fracture conductivity T_F as well as the fracture length $2x_F$ are restricted by a synthetic curve representing the
transient flow rate in the well. The synthetic curve is performed assuming that $p_w = 10^6$ Pa, $p_i = 10^5$ Pa, $k_m = 10^{-18}$ m²,
$T_F = 1.5 \cdot 10^{-16}$ m³, $s_m = 10^{-11}$ Pa⁻¹, $\eta_F = 2.5 \cdot 10^{-4}$ Pa s and $x_F = 23.81$ m (see Fig. 8). The procedure is described in
series of steps as follows:

1. Dimensionally graphing the reciprocal of flow rate vs. time. It is worthwhile noting that the counterclockwise separation of the synthetic curve (red line) from the bilinear-fit-curve (grey line) represents the moment ~~when is exhibited in the well the~~ arrival of the pressure front at the fracture tip, defining the end of bilinear flow.

2. Calculate T_F as is typically done (see, e.g., Guppy et al., 1981b), i.e., based on the slope of bilinear-fit-curve $1/q_w = mt^{1/4}$ (Eq. 12). The dimensional fracture conductivity is determined as follows:

$$T_F = \left(\frac{2.61 \eta_F^{3/4}}{k_m^{1/4} s_m^{1/4} h (p_w - p_i) m} \right)^2. \tag{27}$$

   According to this example, ~~it is obtained~~ $T_F = 1.5 \cdot 10^{-16}$ m³. This value is the same as the one employed to perform the synthetic curve.

3. Read from the graph the termination of bilinear flow defined by the separation of the curve that represents the $1/q_w$ measured in the well (red curve) from the curve proportional to $t^{1/4}$ (grey curve). This time corresponds to the reflection time. In practical terms, it is considered a calculation error in the separation of 5%, which corresponds approximately to the visual estimation of the point at which ~~both~~ curves start departing from each other. In this case study, the reflection time t_r is approximately 10^4 s.

4. Introduce the value of reflection time t_r calculated in the previous step in the relation $\tau_a \cong 0.0736 \tau_r$ and obtain the arrival time of the isobars at the fracture tip. For the example at hand $\tau_a = 736$ s.

5. Determine the value of D_b from its definition:

$$D_b = \frac{T_F^2}{k_m \eta_F s_m}. \tag{28}$$

   For the present case study, taking into account the example and the parameters of the simulation, ~~it is obtained~~ $D_b = 9$ m⁴ s⁻¹.

6. Introduce the value of t_a, obtained at step 4, and the value of D_b, calculated at step 5, in the equation of migration of isobars along the fracture (Eq. 16) and, in this way, calculate the fracture half-length. In this case, the isobar under study is $P_N = 0.05$, as a result the constant $\alpha_b = 2.23$. Utilizing ~~the~~ Eq. (16) ~~documented for the first time in this work~~ we have:

$$x_F = \alpha_b (D_b t_a)^{1/4}. \tag{29}$$

   When introducing the corresponding values of the considered example, ~~it is obtained~~ $x_F = 20.12$ m.

7. Finally, the fracture length is approximately 40.24 m ($2x_F$). It can be noted that this result is slightly lower than 47.62 m, which is the value that denotes the real magnitude used to represent the synthetic curve. It is possible to obtain more accurate results by quantitively calculating the separation between the curves of the considered

example instead of visually estimating it. For instance, when calculating exactly the point at which the separation is 5% it is obtained an arrival time of 865.5 s and a fracture length of 41.9 m.

425 **4.1.2 Case 2: low dimensionless fracture conductivities T_D**

In the case of low T_D, it is not possible to estimate the fracture length utilizing the bilinear flow theory, since this flow regime ends before the isobar at study arrives at the fracture tip. This is expressed in terms of the pressure field by the observation of the premature occurrence of a significant pressure change in the fracture tip. However, it is possible to restrict the minimum fracture length. In the following example, the values of the dimensional fracture conductivity T_F as well as the

430 minimum fracture length $2x_F$ are constrained by a synthetic curve representing the transient flow rate in the well. This latter curve is computed assuming that $p_w = 10^6$ Pa, $p_i = 10^5$ Pa, $k_m = 10^{-18}$ m², $T_F = 1.5 \cdot 10^{-16}$ m³, $s_m = 10^{-11}$ Pa⁻¹, $\eta_F = 2.5 \cdot 10^{-4}$ Pa s and $x_F = 136.36$ m (see Fig. 9). The procedure is outlined in the following steps:

1. Dimensionally graphing the reciprocal of flow rate vs. time.

2. Calculate the value of T_F as commonly conducted in the related literature (See, e.g., Guppy et al., 1981b), i.e., based

435 on the slope of bilinear-fit-curve $1/q_w = mt^{1/4}$ (Eq. 12). The dimensional fracture conductivity is determined as follows:

$$T_F = \left(\frac{2.61\eta_F^{3/4}}{k_m^{1/4} s_m^{1/4} h(p_w - p_i)m} \right)^2. \tag{30}$$

According to this example, it is obtained $T_F = 1.5 \cdot 10^{-16}$ m³. This value is the same as the one used to calculate the synthetic curve.

440 3. Read from the graph the termination of bilinear flow defined by the clockwise separation off the curve that represents the $1/q_w$ measured in the well (blue curve) from the curve proportional to $t^{1/4}$ (grey curve). This time is defined as transition time and it is similar for all cases with low T_D. Similar to the previous case, a calculation error in the separation of 5% is considered, which corresponds approximately to the visual estimation of the point at which both curves start departing from each other. In this example, the transition time t_t is approximately 10^6 s.

445 4. Introduce the value of transition time t_t, calculated in the previous step, in the relation $\tau_a \cong 0.0736\tau_t$ and obtain the fictitious arrival time of the isobars at the fracture tip. For the contemplated case example, $\tau_a = 73600$ s.

5. Determine the value of D_b from its definition:

$$D_b = \frac{T_F^2}{k_m \eta_F s_m}. \tag{31}$$

In the context of the example at hand and considering the parameters of the simulation, it is obtained $D_b = 9$ m⁴ s⁻¹.

6. Introduce the value of $t_{a\star}$ obtained at step 4, and the value of D_b computed at step 5, in the equation of migration of isobars along the fracture (Eq. 16) and, in this way, calculate the fictitious fracture half-length. In this case, the isobar under study is $P_N = 0.05$, as a consequence the constant $\alpha_b = 2.23$. Utilizing ~~the~~ Eq. (16) ~~documented for the first time in this work~~ we have:

$$x_F = \alpha_b (D_b t_a)^{1/4}. \tag{32}$$

When incorporating the corresponding values of this example, it is obtained $x_F = 63.62$ m.

7. Finally, the minimum fracture length is approximately 127.23 m $(2x_F)$, whereas the real value used to represent the synthetic curve is 272.72 m.

In the cases described previously, the practical use of Eq. (16) to constrain the length of a fracture with finite conductivity has been demonstrated by analyzing the transient behavior of flow rate in the well during a hydraulic test at constant pressure.

The expressions obtained in this work for the ending time of bilinear flow, the pressure propagation and the bilineal diffusivity D_b, complement the limited theory that exists about data analysis from wells producing or injecting at constant pressure. The clarity and simplicity of these equations allows these to be used quickly to estaimate the length of fractures with finite conductivity. The bilineal diffusivity D_b, firstly introduced by Ortiz R. et al. (2013) for constant well flowrate and demonstrated in this work to also hold for the case of constant well pressure, could in principle be estimated in the laboratory by means of Eq. (16). In addition, this bilineal diffusivity allows, on the one hand, for a relatively uncomplicated comparison beween finite conductivy fractures. On the other hand, these equations could in one way or another be integrated into more general methods such as the transient rate analysis for the interpretation of production data. Finally, the diffusion equations of pressure in the matrix and the fracture (Eqs. 16 and 17) are also useful to reduce the associated risks related to induced seismicity generated by changes of pressure in fractured reservoirs or faults, as a consequence of massive fluid injection (e.g. Shapiro, 2015; Shapiro and Dinske, 2009). By knowing and understanding the physics behind the migration of isobars it is possible to minimize the associated risks with changes in pores pressure.

5 Conclusion

The results of our study suggest that the reciprocal of dimensionless flow rate $1/q_{wD}$ is proportional to the fourth root of dimensionless time τ during the bilinear flow regime for the case of injection at constant pressure in the well. Previously, Guppy et al. (1981b) obtained the factor $A = 2.722$ (Eq. 10), which is slightly greater than the factor obtained here $A = 2.60$ (Eq. 12). This discrepancy is attributed to our finer spatial and temporal discretization in comparison with the discretization used by Guppy et al. (1981b).

During bilinear flow regime the migration of isobars along the fracture is described as: $x_i(t) = \alpha_b (D_b t)^{1/4}$, where $D_b = T_F^2 / k_m \eta_f s_m$ (m^4 s^{-1}) is defined in the same way as in Ortiz R. et al. (2013) as the effective hydraulic diffusivity of fracture

during bilinear flow regime. Moreover, the migration of isobars in the matrix is given by: $y_i(t) = \alpha_m(D_m t)^{1/2}$, where $D_m = k_m/(\eta_f s_m)$ (m^2 s^{-1}) denotes the hydraulic diffusivity of matrix.

As for the ~~transient~~ of flow rate in the well, the termination of bilinear flow is given by (a) the transition time τ_t (circumferences in Fig. 7 and Eq. 20), valid for low T_D and (b) the reflection time τ_r (squares in Fig. 7 and Eq. 21), valid for high T_D.

When it comes to the propagation of isobars along the fracture, the termination of bilinear flow is given by (a) the fracture time τ_F (filled circles in Fig. 7 and Eq. 22), valid for low T_D and (b) the arrival time τ_a (triangles in Fig. 7), valid for high T_D.

Similarly as in Ortiz R. et al. (2013), it was observed that isobars accelerate when they approach to the fracture tip (Figs. 3 and 5). This acceleration was verified by studying the velocity of isobars using the graphs v_{iD} vs. τ and v_{iD} vs. x_{iD} (Fig. 6). It was concluded that for a fixed dimensionless position in the fracture x_{iD}, the velocity v_{iD} is higher for low values of normalized isobars p_N as well as for high fracture conductivities T_D (see Figs. 6b and 6d).

In a follow-up study, it would be interesting to include the effect of fracture storativity and investigate, utilizing an analogue method to that discussed in this work, the behavior of a fracture with conductivity high enough to lead to fracture and formation linear flow.

Author contribution

Patricio I. Pérez D. was responsible for numerical model and simulations, analysis of results, preparation of the draft and final paper. Adrián E. Ortiz R. contributed the theoretical underpinning, presentation of results, preparation of the draft and final paper. Ernesto Meneses Rioseco contributed the theoretical underpinning in composing the numerical model, analysis of results and preparation of the final paper.

Acknowledgments

It was possible to complete this work only through the international collaboration between the Department of Chemical and Environmental Engineering - Universidad Técnica Federico Santa María (Chile) and the Department of Geothermics and Information Systems - Leibniz Institute for Applied Geophysics (Germany).

Competing interests

The authors declare that they have no conflict of interests.

Nomenclature

A	constant, Eq. (12)
b_F	aperture of fracture, m
c_a	coefficient of fit equation for the arrival time, Table 1 and Fig. 7
c_r	coefficient of fit equation for the reflection time, Table 1 and Fig. 7
c_t	coefficient of fit equation for the transition time, Table 1 and Fig. 7
D_b	effective hydraulic diffusivity of fracture during bilinear flow regime, Eq. (16), $m^4\,s^{-1}$
D_m	hydraulic diffusivity of matrix, Eq. (17), $m^2\,s^{-1}$
$f(t_D)$	transient behavior of pressure in the well, Eq. (11), Pa
h	height of the open well section, fracture height, Eq. (5), m
k_F	fracture permeability, m^2
k_m	matrix permeability, m^2
p_i	initial pressure of matrix and fracture, Eq. (5), Pa
P_N	normalized pressure difference, Eq. (13)
p_w	constant injection pressure, Eq. (5), Pa
$p(x,y,t)$	pressure at the position (x,y) in the fracture or the matrix at time t, Eq. (13), Pa
q_w	flow rate in the well, Eq. (5), $m^3\,s^{-1}$
q_{wD}	dimensionless flow rate in the well, Eq. (5)
q_{wDt}	dimensionless flow rate of type-curves, Eqs. (20) and (21), Fig. 2
$q_{wD\infty}$	dimensionless flow rate of the master curve, Eq. (21), Fig. 2
$q_F(x,t)$	fluid flow between matrix and fracture, $m^2\,s^{-1}$
s_F	specific storage capacity of fracture, Pa^{-1}
s_m	specific storage capacity of matrix, Pa^{-1}
t	dimensional time, Eq. (7), s
t_a	dimensional arrival time, s
t_D	conventional dimensionless time, Eq. (7)
T_D	dimensionless fracture conductivity, Eq. (6)
T_F	fracture conductivity, Eq. (6), m^3
v_{iD}	dimensionless velocity of isobars along the fracture, Eqs. (18) and (19)
x,y	spatial coordinates along, normal to the fracture with origin at the well, Eqs. (8) and (9), respectively, m
x_F	fracture half-length, Eq. (6), m

x_D, y_D	dimensionless coordinates, Eqs. (8) and (9), respectively
x_{iD}, y_{iD}	dimensionless distances of isobars from the well (along the x_D and y_D axis, Eqs. (14) and (15), respectively
x_{iDf}	dimensionless propagation of migration-fit-curves, Eq. (22), Fig. 3
x_{iDt}	dimensionless propagation of migration-type-curves, Eq. (22), Fig. 3
α_b	constant for pressure diffusion in the fracture during bilinear flow, Eqs. (14) and (16)
α_m	constant for pressure diffusion in the matrix, Eqs. (15) and (17)
β_b	constant for velocity in the fracture depending on time, Eq. (18)
γ_b	constant for velocity in the fracture depending on space, Eq. (19)
Δ	constant, Eq. (11)
ε	quantification of error in the termination of bilinear flow, Eqs. (20), (21) and (22), Fig. 7
η_f	dynamic fluid viscosity, Pa s
τ	dimensionless time, Eq. (5)
τ_a	dimensionless arrival time, Fig. 7
τ_F	dimensionless fracture time, Fig. 7
τ_r	dimensionless reflection time, Fig. 7
τ_t	dimensionless transition time, Fig. 7

References

Arps, J.J.: Analysis of Decline Curves, Trans. AIME, 160, 228–247, https://doi.org/10.2118/945228-G, 1945.

Agarwal, R.G., Carter, R.D., Pollock, C.B.: Evaluation and Performance Prediction of Low-Permeability Gas Wells Stimulated by Massive Hydraulic Fracturing, J. Pet. Technol., 31, 362–372. https://doi.org/10.2118/6838-PA, 1979.

Barenblatt, G., Zheltov, I., Kochina, I.: Basic concepts in the theory of seepage of homogeneous liquids in fissured rocks [strata], J. Appl. Math. Mech., 24, 1286–1303, https://doi.org/10.1016/0021-8928(60)90107-6, 1960.

Basayir Hussain Mohsin Al-Lawati: Use of rate transient analysis to enhance the well perfomance of a mature gas field, Texas A&M University, 2017.

Belyadi, H., Yuyi, S., Junca-Laplace, J.-P.: Production Analysis Using Rate Transient Analysis, in: SPE Eastern Regional Meeting, Society of Petroleum Engineers, Morgantown, West Virginia, 13-15 October, https://doi.org/10.2118/177293-MS, 2015.

Berumen, S., Samaniego, F., Cinco, H.: An investigation of constant-pressure gas well testing influenced by high-velocity

flow, J. Petrol. Sci. Eng., 18, 215–231, https://doi.org/10.1016/S0920-4105(97)00014-4, 1997.

520   Chen, H.-Y., Teufel, L.W.: A New Rate-Time Type Curve for Analysis of Tight-Gas Linear and Radial Flows, in: SPE Annual Technical Conference and Exhibition, Society of Petroleum Engineers, Dallas, Texas, 1-4 October, https://doi.org/10.2118/63094-MS, 2000.

Cinco-Ley, H., Samaniego-V., F.: Transient Pressure Analysis for Fractured Wells, J. Pet. Technol., 33, 1749–1766, https://doi.org/10.2118/7490-PA, 1981.

525   Cinco L., H., Samaniego V., F., Dominguez A., N.: Transient Pressure Behavior for a Well With a Finite-Conductivity Vertical Fracture, Society of Petroleum Engineers Journal, 18, 253–264, https://doi.org/10.2118/6014-PA, 1978.

Da Prat, G.: Well Test Analysis for Fractured Reservoir Evaluation, v. 27., United States, 1990.

Dejam, M., Hassanzadeh, H., Chen, Z.: Semi-analytical solution for pressure transient analysis of a hydraulically fractured vertical well in a bounded dual-porosity reservoir, J. Hydrol., 565, 289–301,
530   https://doi.org/10.1016/j.jhydrol.2018.08.020, 2018.

Earlougher Jr., R.C.: Advances in Well Test Analysis, Henry L. Doherty series; Monograph (Society of Petroleum Engineers of AIME), v. 5., Henry L. Doherty Memorial Fund of AIME, New York, 1977.

Ehlig-Economides, C.A.: Well test analysis for wells produced at a constant pressure, Stanford, 1979.

Escobar, F.-H., Sánchez, J.A., Cantillo, J.H.: Rate transient analysis for homogeneous and heterogeneous gas reservoirs
535   using the TDS technique, C.T.F Cienc. Tecnol. Futur., 3, 45–59, 2008.

Fetkovich, M.J.: Decline Curve Analysis Using Type Curves, J. Pet. Technol, 32, 1065–1077, https://doi.org/10.2118/4629-PA, 1980.

Guppy, K.H., Cinco-Ley, H., Ramey, H.J.: Effect of Non-Darcy Flow on the Constant-Pressure Production of Fractured Wells, Society of Petroleum Engineers Journal, 21, 390–400, https://doi.org/10.2118/9344-PA, 1981a.

540   Guppy, K.H., Cinco-Ley, H., Ramey, H.J.: Transient Flow Behavior of a Vertically Fractured Well Producing at Constant Pressure, Society of Petroleum Engineers Journal, 1981b.

Guppy, K.H., Kumar, S., Kagawan, V.D.: Pressure-Transient Analysis for Fractured Wells Producing at Constant Pressure, SPE Formation Evaluation, 3, 169–178, https://doi.org/10.2118/13629-PA, 1988.

545   He, Y., Cheng, S., Rui, Z., Qin, J., Fu, L., Shi, J., Wang, Y., Li, D., Patil, S., Yu, H., Lu, J.: An improved rate-transient analysis model of multi-fractured horizontal wells with non-uniform hydraulic fracture properties, Energies, 11, 1–17, https://doi.org/10.3390/en11020393, 2018.

Heidari Sureshjani, M., Clarkson, C.R.: Transient linear flow analysis of constant-pressure wells with finite conductivity hydraulic fractures in tight/shale reservoirs, J. Petrol. Sci. Eng., 133, 455–466,
550   https://doi.org/10.1016/j.petrol.2015.06.036, 2015.

Houzé, O., Viturat, D., Ole S., F.: Dynamic Data Analysis System, 2018.

Kutasov, I.M., Eppelbaum, L.V.: Drawdown test for a stimulated well produced at a constant bottomhole pressure, First Break, 23, 25–28, https://doi.org/10.3997/1365-2397.2005003, 2005.

Locke, C.D., Sawyer, W.K.: Constant Pressure Injection Test in a Fractured Reservoir-History Match Using Numerical Simulation and Type Curve Analysis, in: Fall Meeting of the Society of Petroleum Engineers of AIME, Dallas, Texas, 28 September-1 October, 1975.

Nashawi, I.S.: Constant-pressure well test analysis of finite-conductivity hydraulically fractured gas wells influenced by non-Darcy flow effects, J. Petrol. Sci. Eng., 53, 225–238, https://doi.org/10.1016/j.petrol.2006.06.006, 2006.

Nashawi, I.S., Malallah, A.H.: Well test analysis of finite-conductivity fractured wells producing at constant bottomhole pressure, J. Petrol. Sci. Eng., 57, 303–320, https://doi.org/10.1016/j.petrol.2006.10.009, 2007.

Ortiz R., A.E., Jung, R., Renner, J.: Two-dimensional numerical investigations on the termination of bilinear flow in fractures, Solid Earth, 4, 331–345, https://doi.org/10.5194/se-4-331-2013, 2013.

Pratikno, H., Rushing, J.A., Blasingame, T.A.: Decline Curve Analysis Using Type Curves - Fractured Wells, in: SPE Annual Technical Conference and Exhibition, Society of Petroleum Engineers, Denver, Colorado, 5-8 October, https://doi.org/10.2118/84287-MS, 2003.

Samaniego-V., F., Cinco-Ley, H.: Transient Pressure Analysis for Variable Rate Testing of Gas Wells, in: Low Permeability Reservoirs Symposium, Denver, Colorado, 15-17 April, 1991.

Shapiro, S.A.: Fluid-Induced Seismicity, Cambridge University Press, Cambridge, England, 1-276, 2015.

Shapiro, S.A., Dinske, C.: Fluid-induced seismicity: Pressure diffusion and hydraulic fracturing, Geophysical Prospecting, 57, 301–310, https://doi.org/10.1111/j.1365-2478.2008.00770.x, 2009.

Silva-López, D., Solano-Barajas, R., Turcio, M., Vargas, R.O., Manero, O., Balankin, A.S., Lira-Galeana, C.: A generalization to transient bilinear flows, J. Petrol. Sci. Eng., 167, 262–276, https://doi.org/10.1016/j.petrol.2018.03.109, 2018.

Torcuk, M.A., Kurtoglu, B., Fakcharoenphol, P., Kazemi, H.: Theory and Application of Pressure and Rate Transient Analysis in Unconventional Reservoirs, in: SPE Annual Technical Conference and Exhibition, Society of Petroleum Engineers, New Orleans, Louisiana, 30 Sep.- 2 Oct., https://doi.org/10.2118/166147-MS, 2013.

Wang, M., Fan, Z., Xing, G., Zhao, W., Song, H., Su, P.: Rate decline analysis for modeling volume fractured well production in naturally fractured reservoirs, Energies, 11, 1-21, https://doi.org/10.3390/en11010043, 2018.

Wattenbarger, R.A., El-Banbi, A.H., Villegas, M.E., Maggard, J.B.: Production Analysis of Linear Flow Into Fractured Tight Gas Wells, in: SPE Rocky Mountain Regional/Low-Permeability Reservoirs Symposium, Society of Petroleum Engineers, Denver, Colorado, 5-8 April, https://doi.org/10.2118/39931-MS, 1998.

Weir, G.J.: Single-phase flow regimes in a discrete fracture model, Water Resources Research, 35, 65–73, https://doi.org/10.1029/98WR02226, 1999.
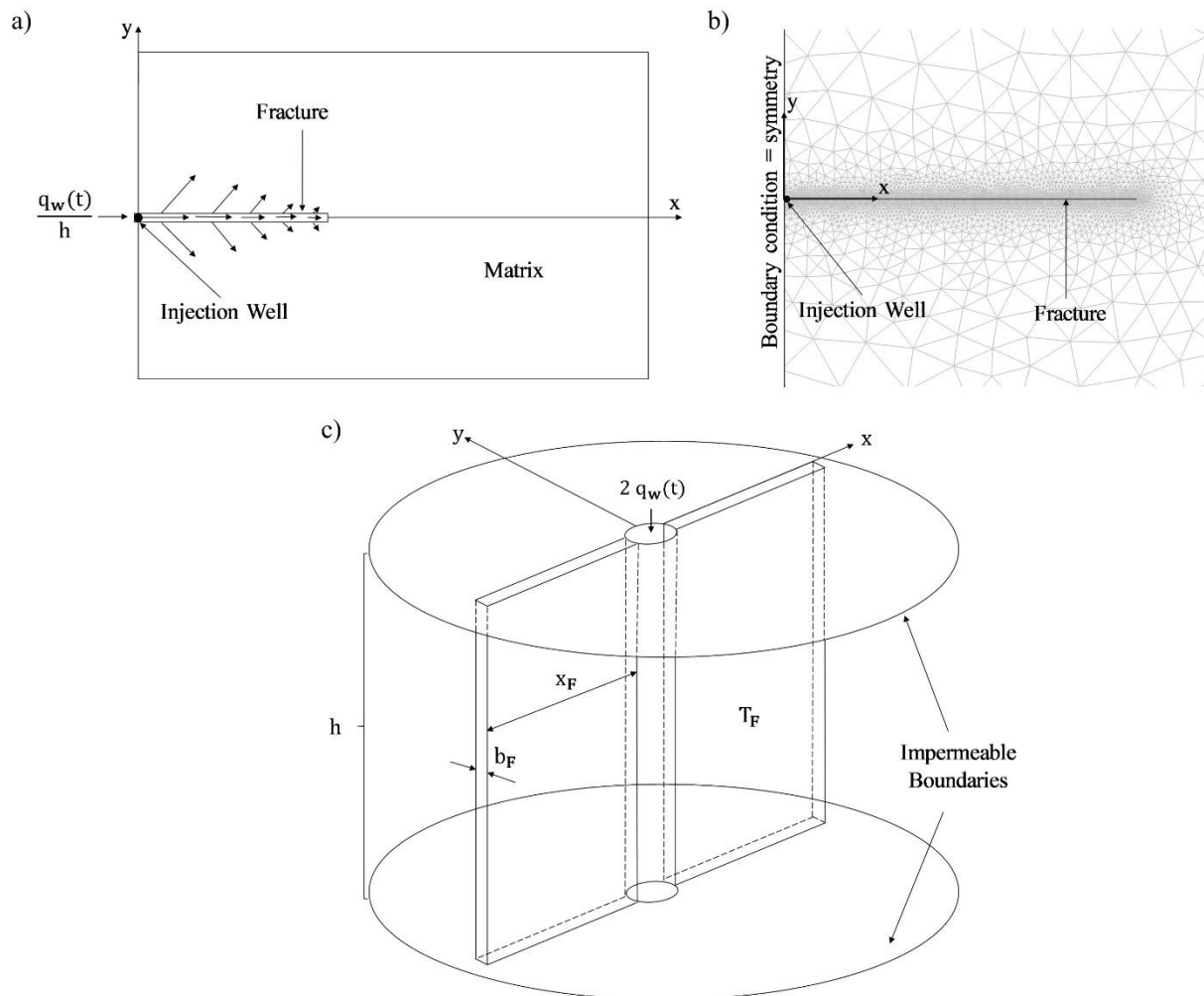
585

Figure 1: (a) 2D representation of model structure; (b) utilized mesh for simulation; and (c) 3D representation of model structure.
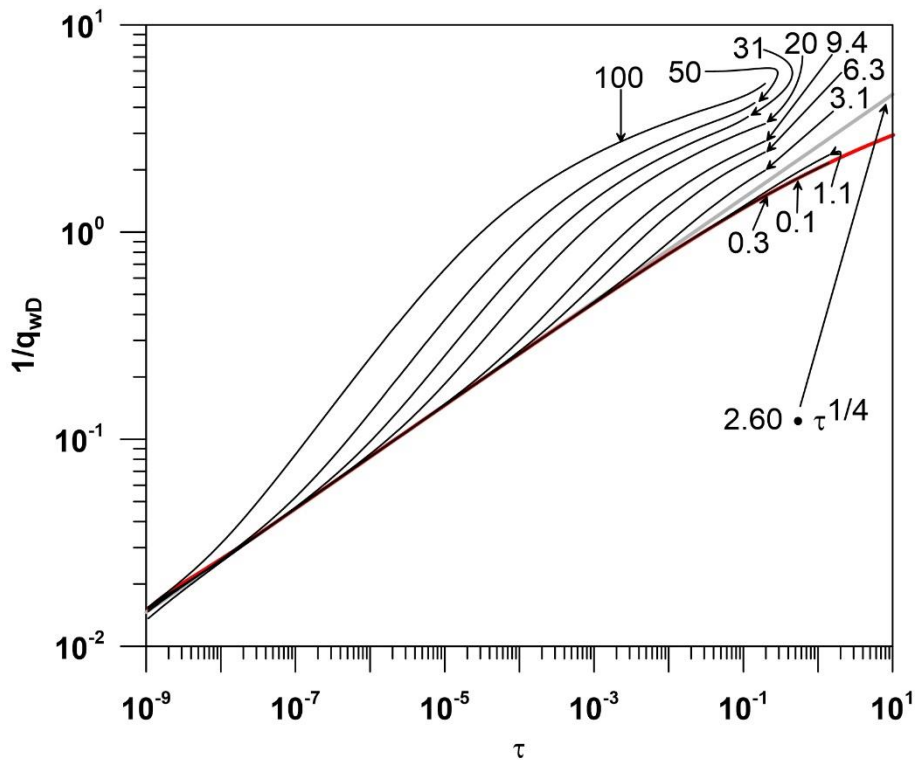
Figure 2: Model results displayed as $1/q_{wD}$ vs. τ in log-log scale. Bilinear-fit-curve (grey line), master curve (red line) and type-curves (black lines).
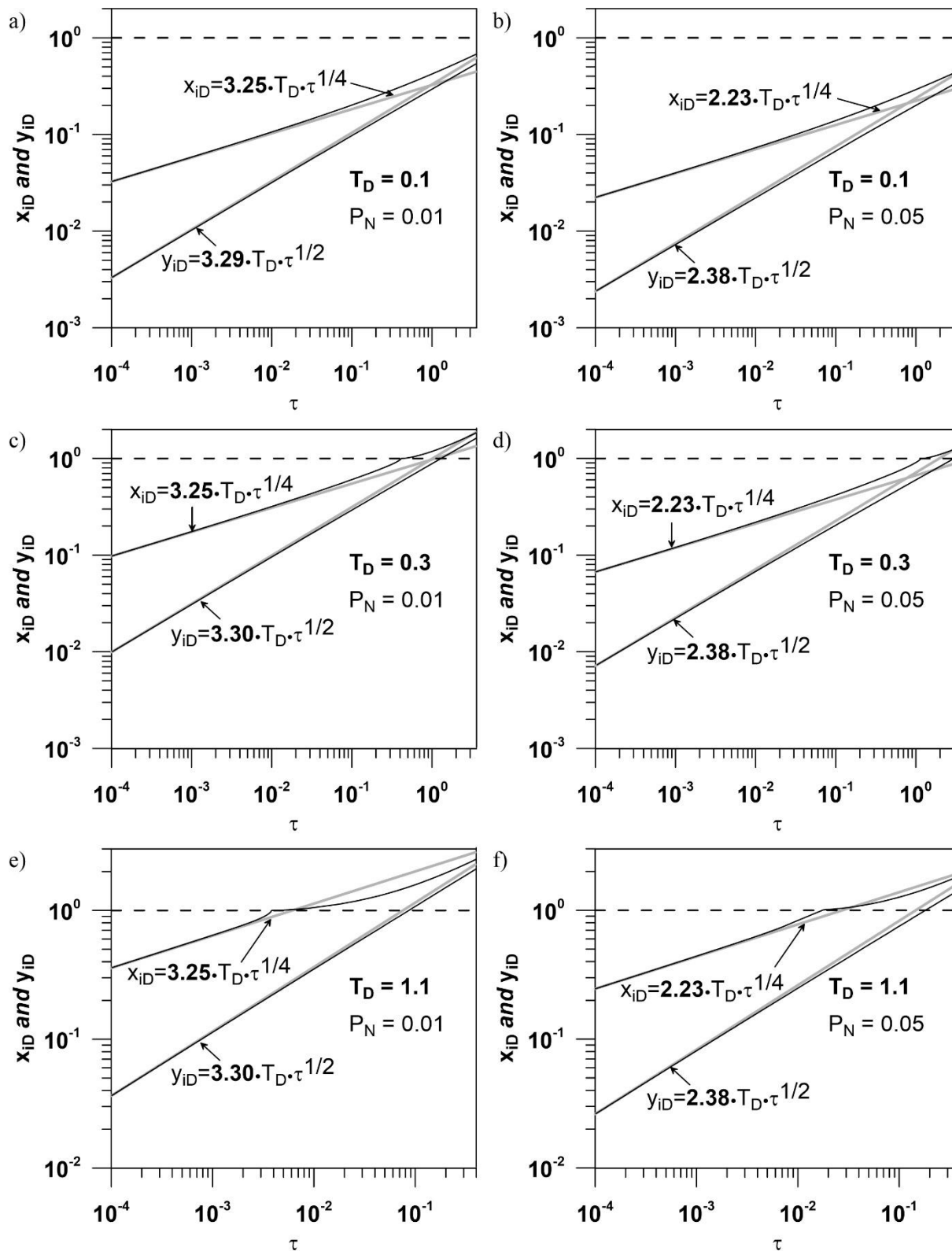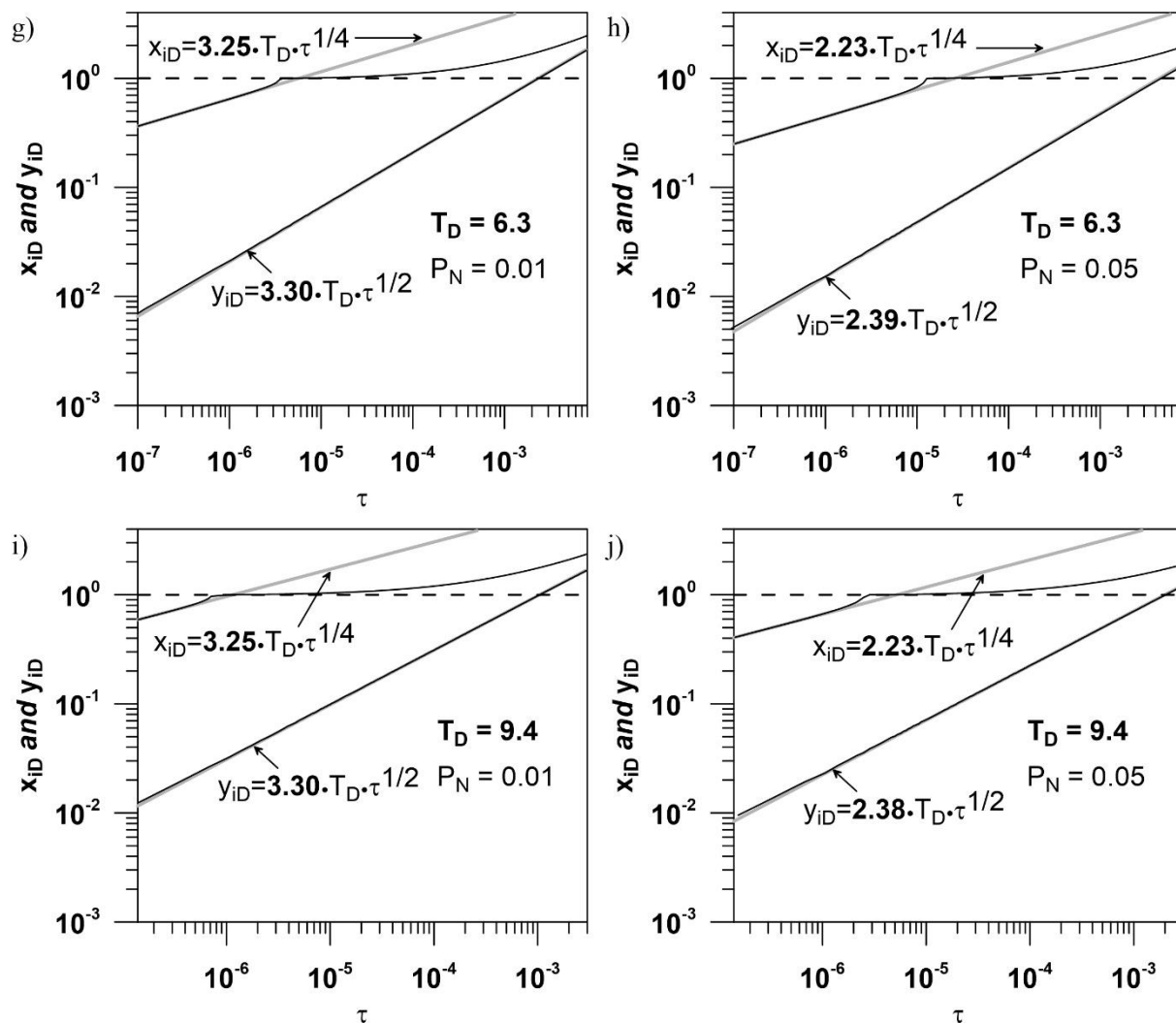
Figure 3: Model results display x_{iD} and y_{iD} vs. τ in log-log scale. Propagation of isobars $P_N = 0.01$ (a, c, e, g, i) and $P_N = 0.05$ (b, d, f, h, j) along the fracture and the formation considering the following fracture conductivities: $T_D = 0.1$ (a, b), 0.3 (c, d), 1.1 (e, f), 6.3 (g, h) and 9.4 (i, j). The dashed lines represent the arrival at the fracture tip of the specific isobars indicated in the graphs.
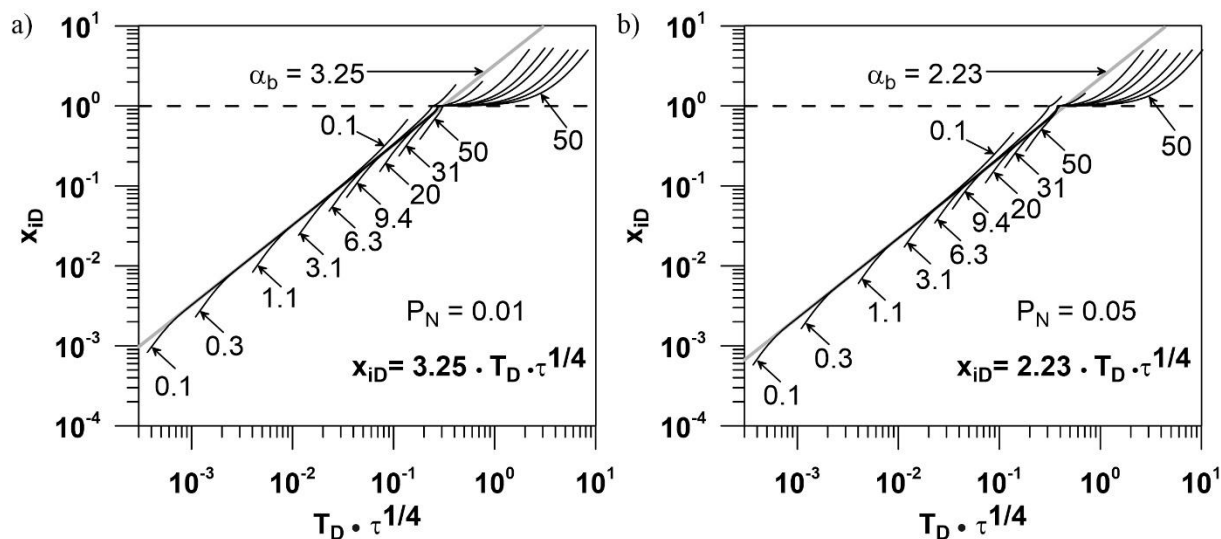
595

Figure 4: Model results in terms of x_{iD} vs. $T_D \cdot \tau^{1/4}$ in log-log scale. Propagation of isobars P_N along the fracture considering the following fracture conductivities: $T_D = 0.1, 0.3, 1.1, 3.1, 6.3, 9.4, 20, 31$ and 50. (a) Model scenarios with $P_N = 0.01$ and $\alpha_b = 3.25$; (b) model scenarios with $P_N = 0.05$ and $\alpha_b = 2.23$. The dashed lines represent the arrival at the fracture tip of the specific isobars indicated in the graphs.

600
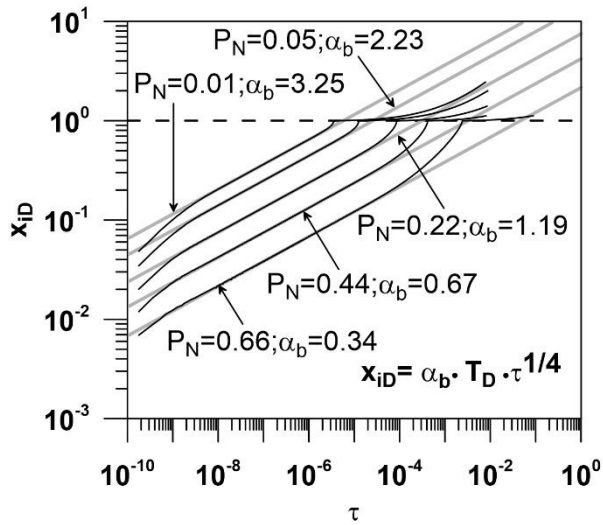
Figure 5: Modeling results in terms of x_{iD} vs. τ in log-log scale. Propagation of isobars $P_N = 0.01, 0.05, 0.22, 0.44$ and 0.66 with $T_D = 6.3$. The dashed line represents the arrival at the fracture tip of the specific isobars indicated in the graph.

605
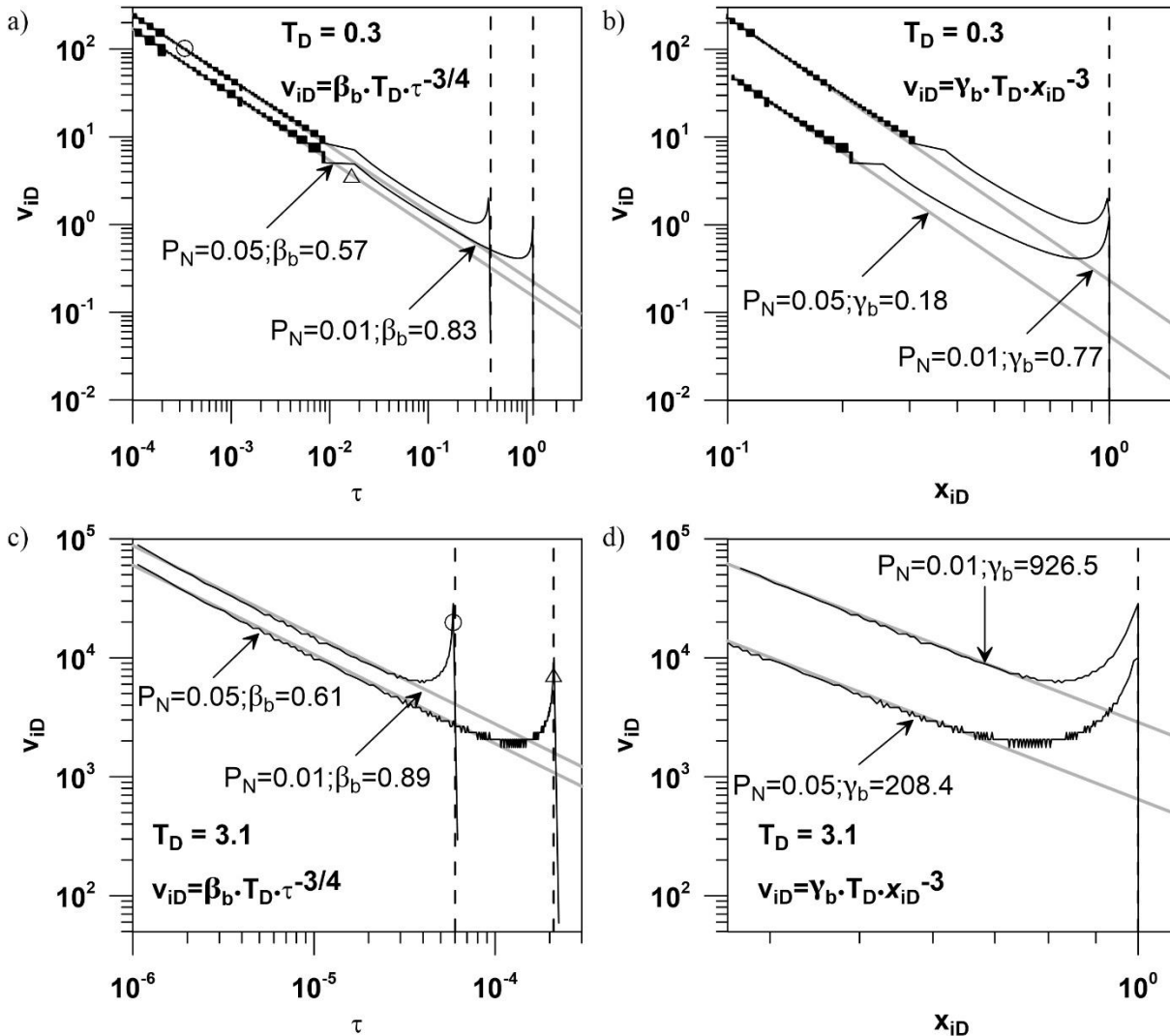
Figure 6: Model results showing v_{iD} **vs.** τ **and** v_{iD} **vs.** x_{iD} **in log-log scale. Velocity of isobars** $P_N = 0.01$ **and** 0.05 **considering** $T_D = 0.3$ **(a, b) and** 3.1 **(c, d). The dashed lines represent the arrival of the specific isobars at the fracture tip. (a) The circle and triangle symbols represent the transition time** τ_t **for** $P_N = 0.01$ **and** 0.05, **respectively (see Eq. 20). (c) The circle and triangle symbols represent the arrival time** τ_a **for** $P_N = 0.01$ **and** 0.05, **respectively (see Fig. 7).**
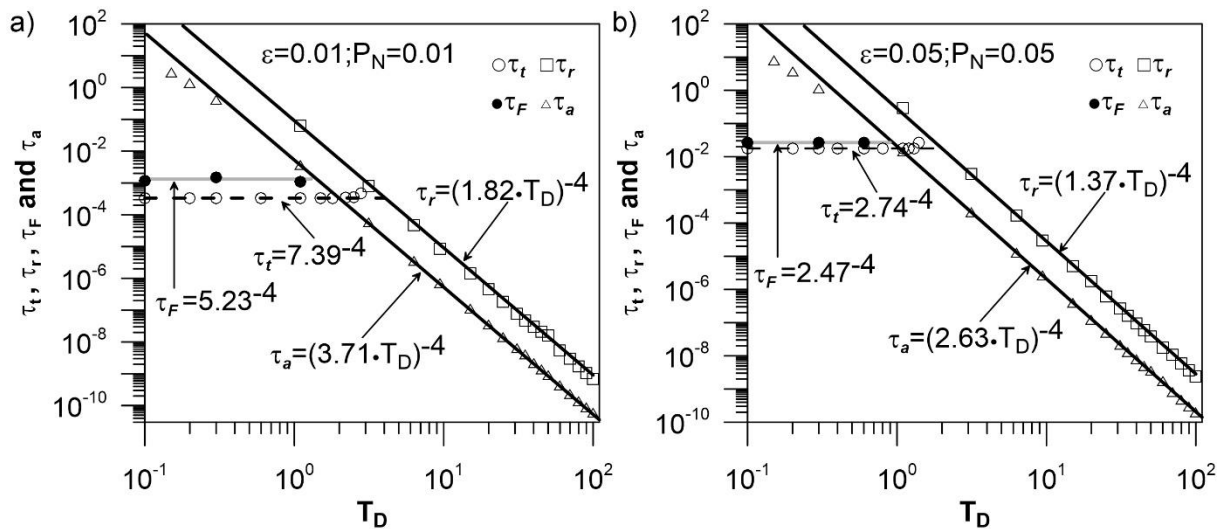
615 **Figure 7: Model results displaying τ_t, τ_r, τ_F and τ_a vs. T_D in log-log scale. τ_t, τ_r, τ_F and τ_a denote the transition time, the reflection time, the fracture time and the arrival time, respectively. The fit-curves for reflection time and arrival time are represented by black lines, for transition time by dashed lines and for fracture time by grey lines. (a) Numerical simulations with ε and $P_N =$ 0.01; and (b) numerical simulations with ε and $P_N = 0.05$ (see Eqs. 20, 21 and 22).**
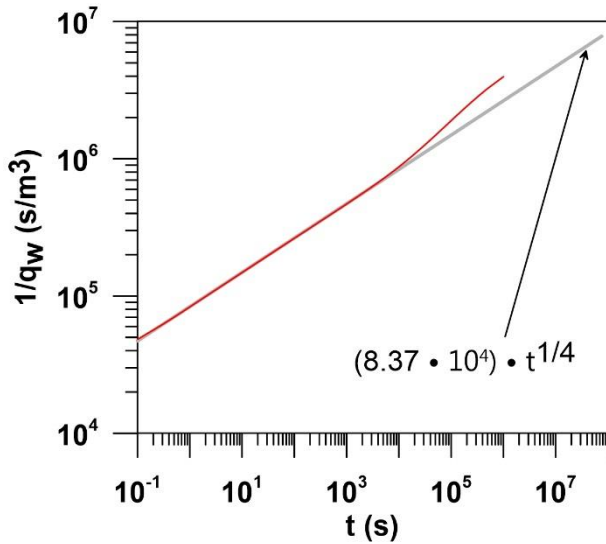
620

Figure 8: $1/q_w$ (s m⁻³) vs. t (s) in log-log scale. The synthetic curve is represented by the red line and the bilinear-fit-curve is displayed with the grey line.
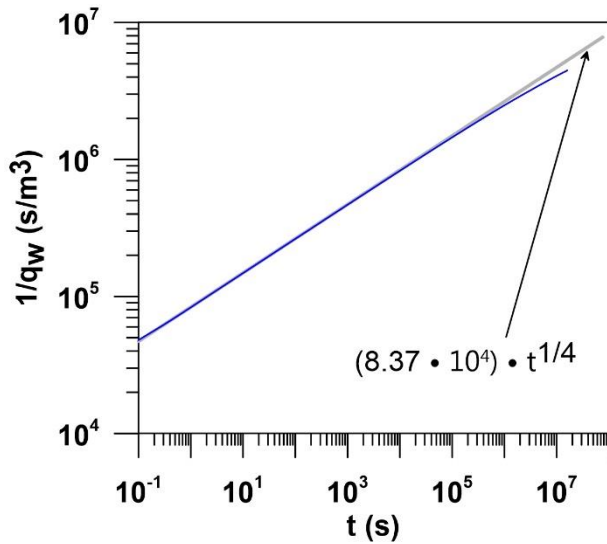
625

Figure 9: $1/q_w$ (s m⁻³) vs. t (s) in log-log scale. The synthetic curve is represented by the blue line and the bilinear-fit-curve is indicated with the grey line.

Paper	Coefficient	With ε and $P_N = 0.01$	With ε and $P_N = 0.05$
Ortiz R. et al. (2013)	c_a	3.40	2.49
	c_r	1.73	1.25
	c_t	6.44	2.53
This work	c_a	3.71	2.63
	c_r	1.82	1.37
	c_t	7.39	2.74

630 **Table 1: Comparison of coefficients of fit equations for the arrival time, the reflection time and the transition time, which have the form $\tau_a = (c_a \cdot T_D)^{-4}$, $\tau_r = (c_r \cdot T_D)^{-4}$ and $\tau_t = (c_t)^{-4}$, respectively.**

Case	Termination time	With ε and $P_N = 0.01$	With ε and $P_N = 0.05$
I	τ_t	$T_D < 2$	$T_D < 1.1$
	τ_r	$T_D > 3$	$T_D > 2$
II	τ_F	$T_D < 1.2$	$T_D < 0.9$
	τ_a	$T_D > 1.2$	$T_D > 0.9$

Table 2: Criteria utilized to calculate the termination of bilinear flow. See discussion for the definition of the case I and II.